Journal of Power Sources 196 (2011) 10667–10672

Contents lists available at SciVerse ScienceDirect

Journal of Power Sources

journal homepage: www.elsevier.com/locate/jpowsour

Mechanism of lithium storage in Si–O–C composite anodes

Xiang Liu*, Man-Chun Zheng, Kai Xie

Department of Material Science and Applied Chemistry, National University of Defense Technology, Changsha 410073, People's Republic of China

ARTICLE INFO

Article history:
Received 27 June 2011
Received in revised form 6 August 2011
Accepted 17 August 2011
Available online 24 August 2011

Keywords:
Lithium anodes
Polymer-derived ceramics
Silicon oxycarbide
Mechanism of lithium storage

ABSTRACT

A Si–O–C composite material is prepared by pyrolyzing a copolymer of phenyl-substituted polysiloxane and divinylbenzene at 800 °C under a hydrogen atmosphere. The material has a high delithiation capacity about 965.3 mA h g^{-1} in the first cycle and retains 660 mA h g^{-1} after 40 cycles at 50 mA g^{-1}. The differential capacity curves of the anode show that there are several reduction peaks between 0.2 and 0.6 V existing all the time during repeated cycles. By comparing ^{29}Si nuclear magnetic resonance (^{29}Si MAS NMR), Si (2p) X-ray photoelectron spectroscopy (XPS) of the anode in the original, fully lithiated, and fully delithiated state, the reduction peaks are related to lithium reversible insertion into SiO_2C_2, SiO_3C, and SiO_4 units, respectively. The corresponding ^{29}Si MAS NMR resonances shift to high field and their binding energies of the Si (2p) XPS peak increase in the fully lithiated state, and then both turn to the opposite direction in the fully delithiated state. The SiO_4 units decrease during repeated cycles. The remaining ones can reversibly transform to Li–silicate (Li_2SiO_3) when lithium is inserted, while the lost ones irreversibly transform to Li–silicate (Li_4SiO_4). However, the $SiOC_3$ units of the material are totally irreversible with lithium because they nearly disappear in the first discharge process, and lead to the formation SiC_4 units.

1. Introduction

Rechargeable lithium-ion batteries are promising power source in consumer electronic devices, such as cell phones and portable computer. However, a conventional anode material, graphite, almost attains its theoretical capacity (372 mA h g^{-1} in the form of LiC_6). Much effort has been paid to create new anode materials to replace graphite, improving the performances such as energy density and cycling of the anodes. Among several alternatives, silicon oxycarbide (Si–O–C) composite materials can be viable anode material. Dahn et al. first studied the possibility to use silicon oxycarbide (Si–O–C) as anode material [1–5]. It was found the Si–O–C composite materials (without Si–Si bonds) can be the origin of capacity, and the content of oxygen resulted in a large irreversible capacity. Later, different silicon containing polymers were pyrolyzed by a variety of researchers [6–12] to produce Si–O–C composite material. According to these previous works, Si–O–C composite materials have been shown to offer higher capacities than graphite. Meanwhile, several other researchers devoted some efforts to the study of the mechanism of the reversible interactions of Si–O–C composite materials and lithium ions in the electrochemical process. Ahn and Raj [13] initially made thermodynamic measurements pertaining to the hysteretic intercalation of lithium and attributed hysteresis partly to the kinetics of lithium diffusion into the Si–O–C particles, and thermodynamic limitations. Fukui et al. [8] employed ^{7}Li NMR to explain the origin of electrochemical lithium storage in Si–O–C composite materials. Three electrochemically active sites were observed: interstitial spaces or edges of the graphene layers, directly or indirectly the Si–O–C glass phase, and the micropores. The first site was thought to contribute the major part of the reversible capacity. However, the above results may not always be the truth because the free carbon content in the Si–O–C composite material does not necessarily exceed 65 wt% ($SiO_{0.51}C_{7.78}$). Further efforts are still needed to devote to the study of mechanism of lithium storage in Si–O–C composite anodes.

A Si–O–C composite material usually consists of (1) free carbon and (2) Si–O–C glass phase. The free carbon forms a continuous matrix and the Si–O–C glass phase is embedded in the carbon matrix. Its nanostructure can be expressed by nanodomain model [14]. The nanodomain model of the Si–O–C composite material is constructed from three components: silica tetrahedral SiO_2 that forms the heart of the domain, and mixed bonds of Si, C, and O in the type SiC_nO_{4-n} (where $0 < n \leq 4$) in the domain walls, and graphene that encases the domains. The first two components show the structures of Si–O–C glass phase, which are expected to electrochemically store lithium species. To produce high capacity Si–O–C material, a phenyl-substituted and branched polysiloxane was employed as the silicon source, and divinylbenzene (DVB) was used as the carbon source. Si–O–C composite material was formed by pyrolyzing copolymer of the polysiloxane and DVB at 800 °C in

* Corresponding author. Tel.: +86 731 8457 3149; fax: +86 731 8457 3150.
E-mail address: hu_nan_xiang@yahoo.com.cn (X. Liu).

0378-7753/$ – see front matter © 2011 Elsevier B.V. All rights reserved.
doi:10.1016/j.jpowsour.2011.08.072

a hydrogen atmosphere. The pyrolysis product was known for its fascinating physical properties [15]. Mechanism of lithium storage in Si–O–C glass phase of the Si–O–C composite material was further proposed by comparing ^{29}Si magic angle spinning nuclear magnetic resonance (^{29}Si MAS NMR) spectroscopy, X-ray photoelectron spectroscopy (XPS) of the material in the original state, fully lithiated state, and fully delithiated state.

2. Experimental

2.1. Synthesis of anode powder

Polysiloxane $Si(CH_3)_3(Si(OH)(CH_3)O)_i(Si(C_6H_5)(CH_3)O)_j(Si(CH_3)(H)O)_k(Si(CH_3)Si(C_3H_7)_2O)_lSi(CH_3)_3$ (where, i, j, k, $l > 1$) and DVB were dissolved in toluene at 100 °C and then gently mixed with a rotary evaporator for 60 min. After evaporation of toluene, it was crosslinked at 250 °C for 4 h in air. The resulting samples were placed in an alumina boat and then pyrolyzed in an alumina tube furnace under constant flushing with ultra-high purity hydrogen (Linde, 99.999%) gas. The flush rate maintained was sufficient to prevent the decomposition and redeposition of vapors released during polymer decomposition. The temperature was raised at a rate of 5 °C min^{-1} to the maximum temperature. And then the maximum temperature was maintained for 60 min.

Silicon content of the pyrolysis product was determined by a fusion technique which consisted of converting the solid to a soluble form and analyzing the solute for total silicon with a Varian 715-ES analysis. Carbon content was measured in FlashEA1112 elemental analyzer (Thermo Electron SPA). Oxygen amount was calculated as a difference to 100% assuming to have less than 1 wt.% of H in the material. The silicon, carbon, and oxygen contents of the pyrolyzed composite material at 800 °C under a hydrogen atmosphere were 30%, 42%, and 27% by weight, respectively. The chemical composition was $SiO_{1.5}C_{3.3}$. The amount of free carbon (i.e., that not bound to silicon, or oxygen) in the product is calculated by subtracting the theoretical amount of carbon bound to silicon from the total carbon. The calculated free carbon content is about 39 wt%.

The morphology of the ball-milled powders was examined using a scanning electron microscope (SEM). A NOVA 2000e (Quantachrome) was employed to measure N_2 sorption isotherms at 77.3 K for open-pore characterization. The Brunauer–Emmett–Teller (BET) and Barret–Joyner–Halenda (BJH) methods were used to estimate the BET surface area (S_{BET}) and average pore diameter, respectively.

2.2. Half-cell preparation

Si–O–C composite anodes of about 25 μm thick were prepared by coating slurries of the pyrolyzed powders (80% by weight), acetylene black (10% by weight), and polyvinylidene fluoride (PVDF) dissolved in N-methyl pyrrolidinone on copper foil substrates. After coating, the electrodes were dried overnight at 110 °C in air and then pressed between flat plates at about 15,000 kPa pressure. Coin-type test cells (four for each sample) were constructed from the electrodes. The electrolyte used was 1 M $LiPF_6$, dissolved in a 50/50 (v/v%) mixture of ethylene carbonate (EC) and diethyl carbonate (DEC). A microporous film (Celgard 2400) wetted with the electrolyte was sandwiched between the active electrode and a Li metal foil anode. Cells were assembled in an argon-filled glove box. Electrochemical testing of the cells was performed using constant current cyclers whose currents are stable to ±1%. The cells were placed in thermostats at 30 °C. Cells were discharged first with a constant current of 50 mA g^{-1}. When the cell discharge potential reached zero volt (fully lithiated state), the current direction was reversed and the cells were in the charge mode. Upon current reversal, Li was removed from the active anode. Charging of the cells was considered complete when the cell potential reached 3.0 V (fully delithiated state).

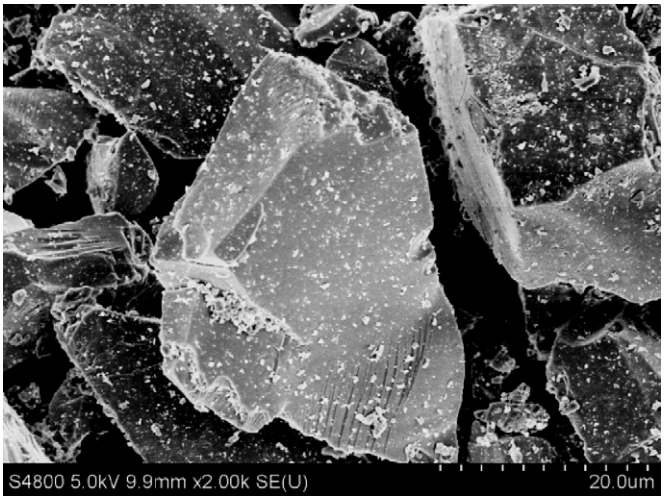

Fig. 1. SEM graph of the prepared Si–O–C composite material under a hydrogen atmosphere.

When cycled 10 times, the Si–O–C composite anodes in the fully lithiated and fully delithiated state were removed in an Ar atmosphere, washed a number of times with DEC, and then dried at room temperature.

XPS spectra of the anodes were recorded using VG Multilab 2000 (Thermo Fisher Scientific). The prepared electrodes were moved into a XPS vacuum chamber without being exposed to the air. Ar gas sputtering was applied to etch away the surface of the anodes to a depth of about 500 nm to eliminate the effect on measurements of the solid electrolyte interface (SEI) layer, or any possible surface contamination. The analysis of the samples yielded values for Si (2p), O (1s).

^{29}Si MAS NMR spectra of the anodes were collected on an AVANCE III spectrometer (Bruker) at 79.49 MHz. A pulse width of 4.50 μt ($\theta = 45°$) and a recycle delay of 30 s were used for single pulse without a cross polarization technique. Samples were finely ground and packed into ZrO_2 rotors (7-mm diam) and spun (6 kHz). All chemical shifts (δ) were referenced to tetramethylsilane (TMS; $\delta = 0$). The experimental spectra were simulated using Origin modeling software.

3. Results and discussion

3.1. Composition and structure

SEM micrograph of the Si–O–C composite material is given in Fig. 1. It can be seen that the composite material is made up of particles that are irregular in shape.

Fig. 2(a) displays the N_2 absorption–desorption isotherms of the prepared Si–O–C composite material. It shows typical reversible type IV isotherms with H1-type hysteresis loop [16]. Fig. 2(b) shows the calculated pore distribution of the material. It is found that most of mesopores diameter was 2–12 nm. The specific surface area calculated with the BET method was 5.1 m^2 g^{-1}, and the average pore diameter calculated with the BJH method was 3.7 nm. The formation of micropores reasonably results from the decomposition and elimination of the polydivinylbenzene or polysiloxane from the composite material. The micropores could maintain cyclability of the Si–O–C anode as alleviative sites for volume change and contribute minor part of the reversible capacity.

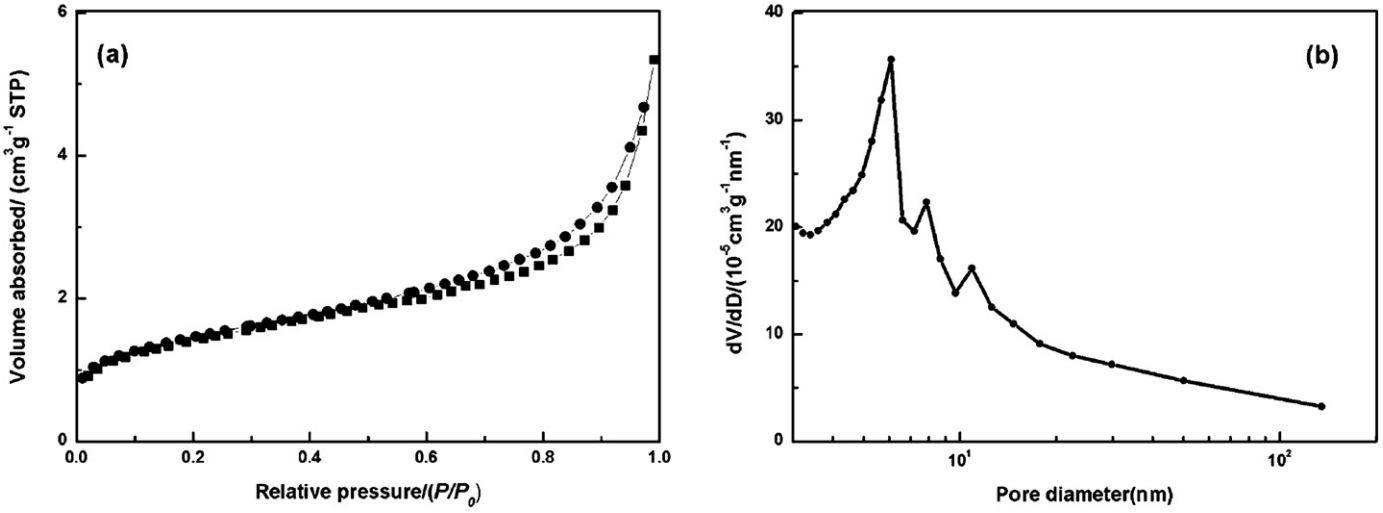

Fig. 2. N_2 absorption–desorption isotherms (a) and pore distribution (b) of the Si–O–C composite material.

The typical lithiation/delithiation profiles of the prepared Si–O–C composite anode are displayed in Fig. 3. The discharge process represents a direction where lithium species are inserted into the Si–O–C composite anode, and the charge process represents the opposite direction. Insertion–extraction cycle exhibits significant hysteresis which may result from the intrinsic polarization within the system. It remains even under equilibrium conditions. Ref. [13] provided possible insights into the origin of the thermodynamic portion of the hysteresis.

As is shown in Fig. 3, the first lithiation capacity is 1643.9 mA h g^{-1} (the chemical composition is $Li_{5.65}SiO_{1.5}C_{3.3}$) and the first delithiation one is 965.3 mA h g^{-1} at 50 mA g^{-1}, leading the first coulombic efficiency to be approximately 57.9%. The cyclic performance of the Si–O–C material is shown in Fig. 4. It can be seen that the delithiation capacity decreases slowly, while it still retains 660 mA h g^{-1} (the chemical composition is $Li_{3.3}SiO_{1.5}C_{3.3}$) after 40 cycles.

Fig. 5 shows the CV (without the first cycle) of the Si–O–C composite anode. For comparison, the CV of commercial amorphous silicon anode and amorphous silicon dioxide anode are also recorded and shown in the same figure. For the Si–O–C anode, a

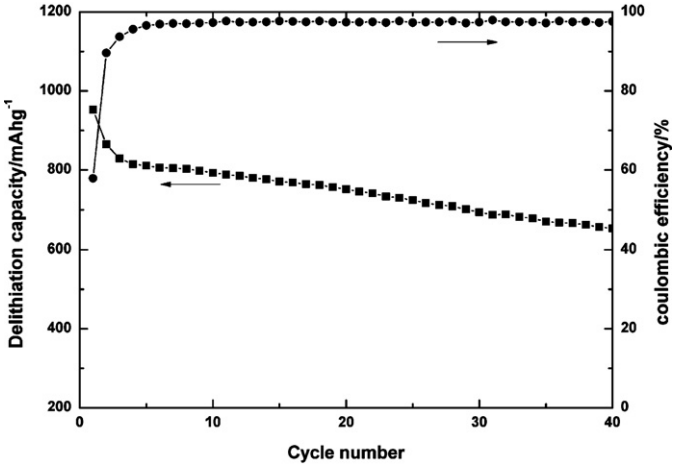

Fig. 4. Cycle performance of the Si–O–C composite anode cycled between 0.001 and 3.0 V (vs. Li/Li^+).

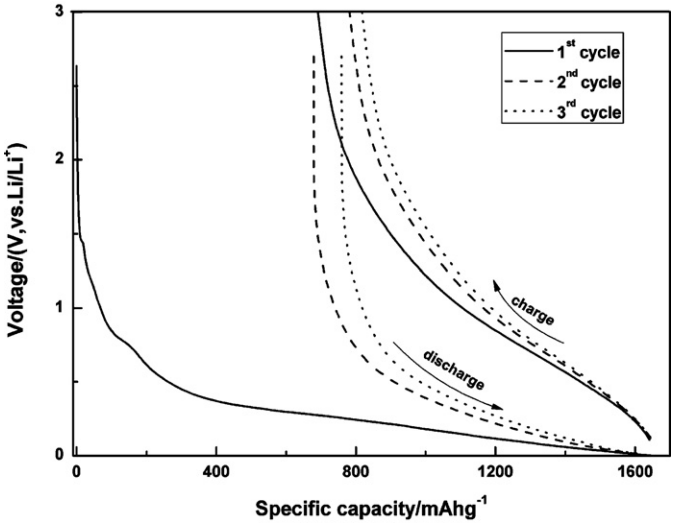

Fig. 3. Charge and discharge profiles of the prepared Si–O–C composite anode in the first three cycles. The charge represents a direction where lithium species are inserted into the Si–O–C composite anodes. The current density is 50 mA g^{-1}.

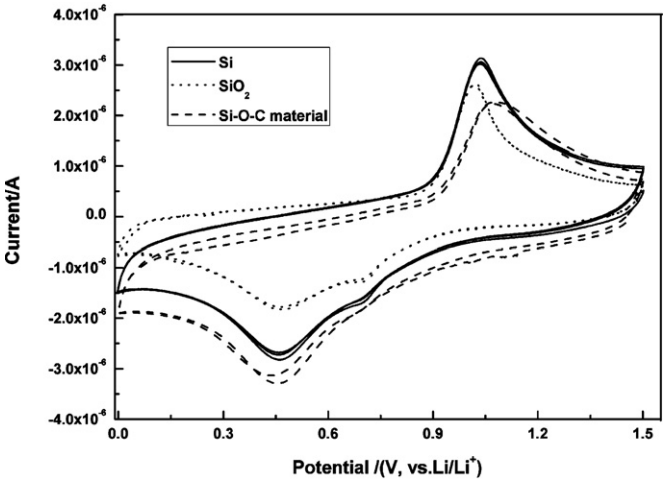

Fig. 5. Cyclic voltammograms of the Si–O–C composite anode recorded in the potential range 0.001–1.5 V at 0.1 mV s^{-1} scan rate (without the first cycle). CV of amorphous silicon and silicon dioxide are shown here for sake of comparison.

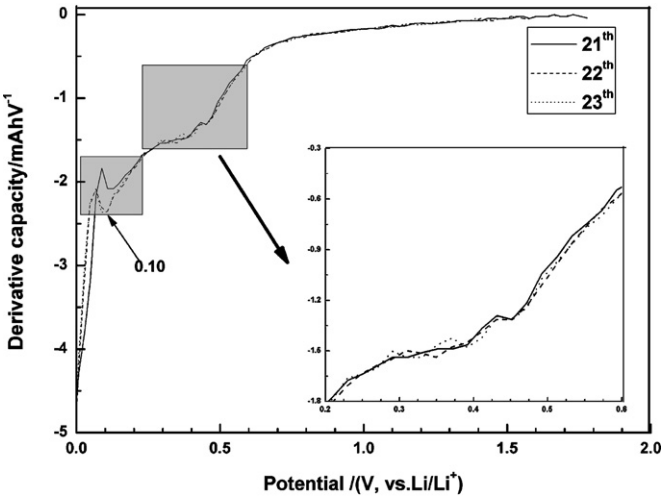

Fig. 6. Differential capacity dQ/dE vs. E profiles in 21th, 22th, and 23th cycle of the Si–O–C composite anode. The profiles contain two regions marked with shadow. The inset graph shows the corresponding profiles between 0.2 and 0.6 V. Peak potentials (V) for stage formation processes are marked.

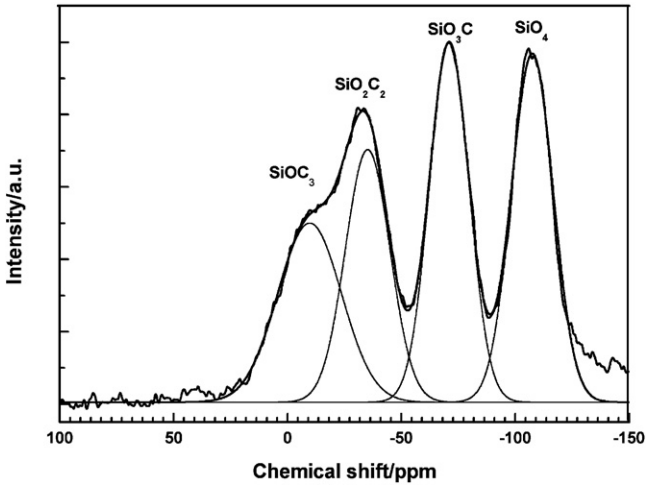

Fig. 7. ^{29}Si MAS NMR of the Si–O–C composite anode in the original state.

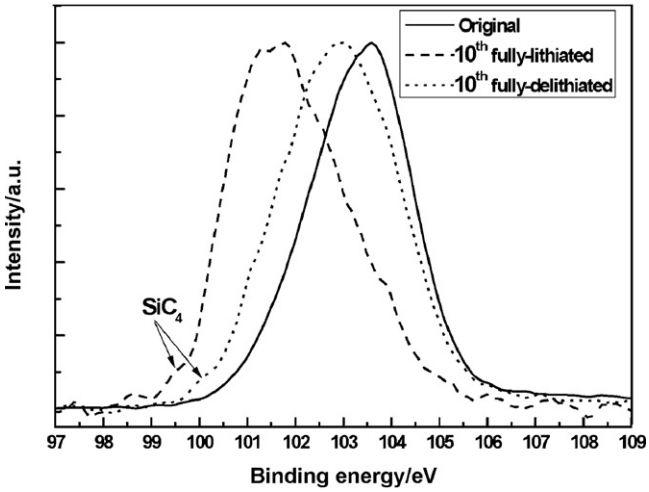

Fig. 8. Si (2p) spectra of the Si–O–C composite anode in the original state, 10th fully lithiated state, and 10th fully delithiated state.

broad peak at approximately 0.49 V retains during repeated cycles, which suggests the presence of a broad band of energy levels for the insertion of lithium ions. Similar peaks at nearly the same potential were observed for commercial amorphous silicon anode and amorphous silicon dioxide anode. It suggests that mechanism of the reactions between lithium and the three anodes may be similar and cannot be distinguished in voltammograms. The minor peak at about 0.60 V could be associated with reactions between lithium and acetylene black, because the peak exists in the CVs of all the three anodes, of which the commercial amorphous silicon anode and amorphous silicon dioxide anode do not have any carbon but acetylene black.

Fig. 6 shows the differential capacity curves of the Si–O–C anode in the 21th, 22th, and 23th cycle. The curves have two characterized regions associated the reversible reaction between lithium and the Si–O–C anode: the first one is at about 0.1 V, corresponding to lithium insertion into micropores as seen in hard carbon [8,17], and the other one is around 0.49 V, which is consistent with the CV analysis. However, it can be seen in the inset graph that the broad 0.49 V peak includes several minor peaks, which are located in the potential range of 0.2–0.6 V. And the associated capacity between 0.2 and 0.6 V accounts for at least 50% of the total reversible capacity. Though the reduction reaction between lithium ions and free carbon is within the potential range, the calculated delithiation capacity from free carbon is much less than the experimental values, since the free carbon only contributes 39 wt% of the total weight. So the broad 0.49 V peak can be mainly related to the formation of Li-alloys due to the reaction between lithium and Si–O–C glass phase [10]. This demonstrates two important facts: (1) the Li-alloy reaction between lithium and Si–O–C glass phase contributes the major part of the reversible capacity, and (2) some silicon species are electrochemically active with lithium ions. It will be seen later that they are corresponding to SiO_2C_2, SiO_3C, and SiO_4.

3.2. Lithium storage in Si–O–C phase

The Si–O–C phase in the Si–O–C composite material is believed to act as a major electrochemically active site for lithium storage. ^{29}Si MAS NMR analysis and Si (2p) XPS spectra were recorded to determine what types of silicon-to-carbon/oxygen coordination are present at different potential state. In the origin state, as is seen in Fig. 7, four ^{29}Si MAS NMR resonances can be seen in the spectrum of the Si–O–C composite anode. They are assigned to SiO_4 (−104 ppm), SiO_3C (−72 ppm), SiO_2C_2 (−34 ppm), and $SiOC_3$ (−5 ppm), respectively. No resonance associated with metallic silicon is observed (−80 ppm) [18]. The presence of SiC_4 is uncertain by overlapping with other peaks. But Si (2p) XPS spectra of the Si–O–C anode in the original state in Fig. 8 show no peaks at 99–100 eV, indicating the absence of SiC_4 units in the material [19]. The absence of SiC_4 is good for the improvement of the reversible capacity because SiC_4 is inactive to lithium ions [2].

The ^{29}Si MAS NMR spectra of the Si–O–C composite anode in the fully lithiated and fully delithiated state in the first and tenth circle are shown in Fig. 9. The data simulated with Lorentzian line are also shown in Fig. 9. It first notices that the resonance of $SiOC_3$ at about −5 ppm disappears in the first discharge process, and never recurs in the following cycles, which suggests that the $SiOC_3$ units irreversibly react with lithium ions and totally contribute the irreversible capacity of the Si–O–C anode. Meanwhile a new resonance at about −20 ppm appears after the first discharge process, and exists all the time in the following charge/discharge cycles. It can be assigned to SiC_4 units[18]. The Si (2p) XPS peak at 99–100 eV in the 10th fully lithiated and fully delithiated state (in Fig. 10) also confirms the existence of SiC_4 units. The resonance of SiC_4 does not significantly shift whatever in the discharge or charge process during repeated cycles (Figs. 9 and 10). It confirms that SiC_4 units

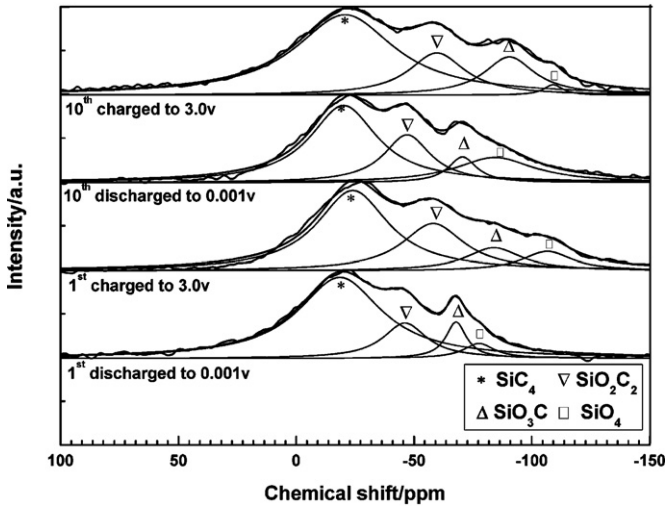

Fig. 9. ^{29}Si MAS NMR of the Si–O–C composite anode in the fully lithiated state and fully delithiated state in the 1st and 10th cycle.

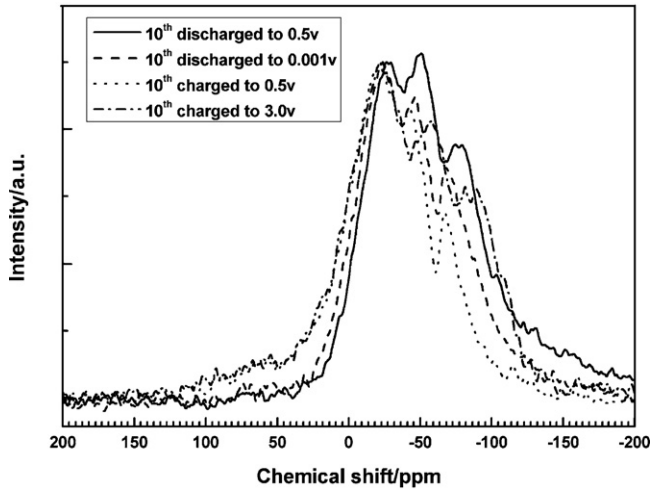

Fig. 10. ^{29}Si MAS NMR of the Si–O–C composite anode at different potential state in the 10th cycle.

are inactive to lithium, which is consistent with the experiment result in literature [2]. The formation of SiC_4 could be associated with the disappearance of $SiOC_3$ units. A proposed mechanism is that lithium ions react with the oxygen atom in $SiOC_3$ units, leading to the formation of Li_2O and SiC_4.

As is also seen in Fig. 9, two resonances are observed at −46 and −68 ppm in the first fully lithiated state, and they shift to −57.6 and −84.7 ppm in the corresponding fully delithiated state. Similar resonances with nearly the same chemical shift are observed in the tenth circle. Fig. 10 shows ^{29}Si MAS NMR spectra of the Si–O–C anode at different potential state in the 10th circle. It can be seen that, the resonances at −46 and −68 ppm in the 10th fully lithiated state gradually reversibly shift to −57.6 and −84.7 ppm during the discharge and charge process, respectively. It indicates that the resonances are corresponding to two associated silicon species reversibly reacting with lithium ions. The insertion of lithium into the Si–O–C phase leads to decrease of the binding energy of Si (2p), confirmed by Si (2p) XPS of the Si–O–C anode in the 10th fully lithiated state in Fig. 8. The ^{29}Si MAS NMR resonances of the material then shift to high field. And the extraction of lithium leads to the increase of the binding energy of Si (2p) and the ^{29}Si MAS NMR resonances shift backward to low field. However, the two

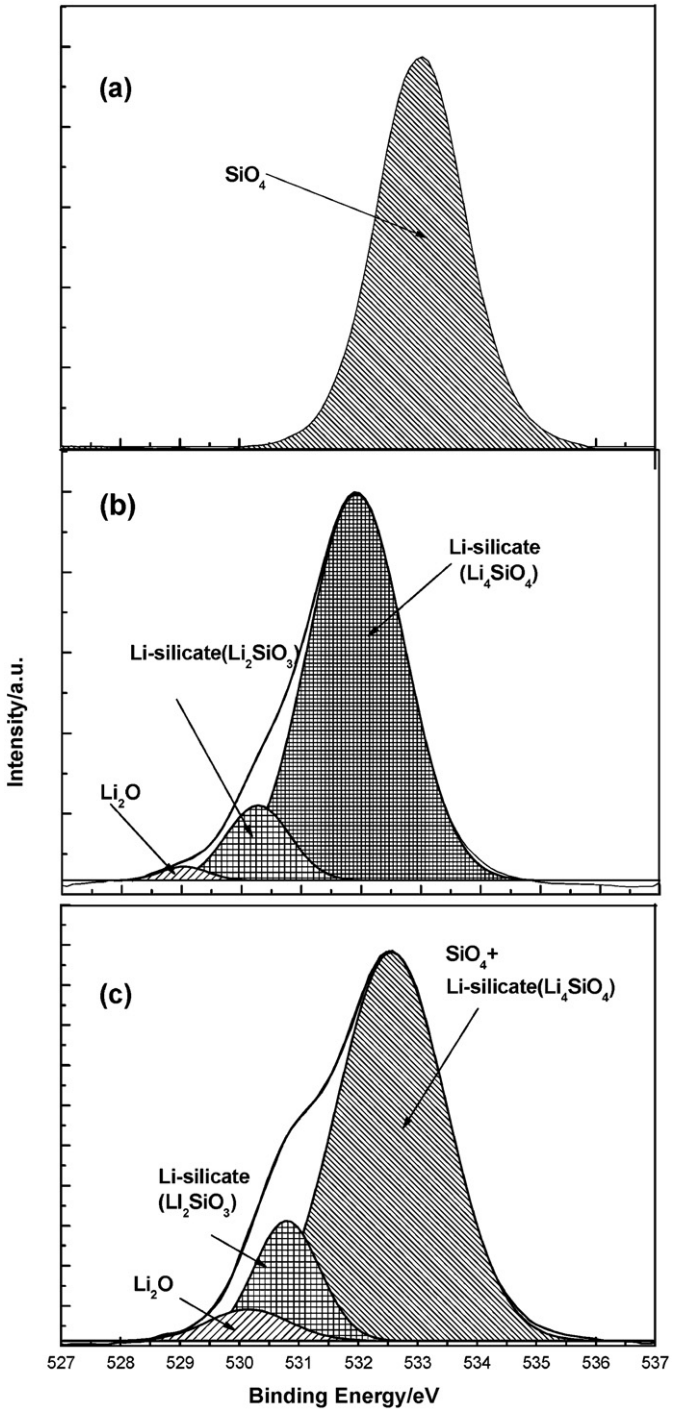

Fig. 11. O (1s) spectra of the Si–O–C composite anode in the original state (a), 10th fully lithiated state (b), and 10th fully delithiated state (c).

resonances, compared with those in the original state, shift to low field in the first fully lithiated state. It could result from the irreversible reaction between lithium and Si–O–C phase. It can also be seen in Fig. 9 the binding energy of these resonances are larger than that of SiC_4, which can be reasonably concluded that the two resonances are corresponding to SiO_2C_2 and SiO_3C units, in which some inactive structures, caused by lithium irreversible insertion, are surely contained.

In addition, a minor resonance is seen at about −84 ppm in the 10th fully lithiated state, and shift to about −105 ppm in the 10th fully delithiated state. The resonances in the fully delithiated state,

Table 1
O (1s) peak attributions for the original state, 10th fully lithiated state, and 10th fully delithiated state of the Si–O–C anode.

Oxygen species	Binding energy (eV)
SiO_2	532.4–532.9
Li_2SiO_3	530.3
Li_4SiO_4	531.8
Li_2O	528.8

compared with that in the original state, can be assigned to SiO_4 units. The resonance at −84 ppm in the 10th fully lithiated state could be assigned to Li–silicate (Li_2SiO_3) [20], which is formed by lithium insertion into SiO_4 units. It is confirmed by O (1s) XPS peak at 530.3 eV in the fully lithiated state [21] (in Fig. 11 and Table 1). The resonance can reversibly shift to the original state when lithium is extracted. It indicates that part of SiO_4 (Li_2SiO_3) could reversibly react with lithium ions. It is also seen that the intensity of the resonance in the tenth cycle is much less than that in the first circle. The lost SiO_4 units could transform to Li_4SiO_4 when reacted with lithium ions, which is confirmed by O (1s) XPS peak at about 531.8 eV in the fully lithiated state [21], though it cannot be distinguished in the ^{29}Si MAS NMR spectra because it is overlapped with the SiO_2C_2 resonance. The Li_4SiO_4 phase still exists in the opposite state, which indicates it contributes the irreversible capacity [22]. It was reported in reference [22] that SiO_2 can reversibly transform to Li–silicate (phyllo, ino). However, the resonances of Li–silicate (phyllo, ino) cannot be distinguished in our ^{29}Si MAS NMR spectra because they are overlapped with other resonances, though their binding energy are close to Li–silicate (Li_2SiO_3).

In conclusion, the $SiOC_3$ units are totally irreversible with lithium. When lithium is inserted, they are transformed to SiC_4 units, which are inactive with lithium. The other three silicon species could reversibly react with lithium, corresponding to the reduction peaks in differential capacity curves of the Si–O–C anode in the 21th, 22th, and 23th cycle. It can be deduced from these facts that not all oxygen species in the Si–O–C anode are irreversible and contribute the irreversible capacity, which was experimentally observed in Si–O–C anodes [10]. In the contrary, the reversible capacity is expected to be rise with an increase of SiO_2C_2 and SiO_3C content with similar experimental condition.

4. Conclusions

A copolymer of phenyl-substituted, branched polysiloxane (containing Si–H bonds) and divinylbenzene was pyrolyzed at 800 °C in a hydrogen atmosphere and transformed to Si–O–C composite anodes for recharge lithium ion batteries. The anodes exhibit high reversible capacity. The first lithiation capacity is 1643.9 mA h g^{-1} and the first delithiation one is 965.3 mA h g^{-1} at 50 mA g^{-1}, leading the first coulombic efficiency to be approximately 57.9%. The reversible capacity still retains 660 mA h g^{-1} after 40 cycles.

Several reduction peaks in the potential range of 0.2–0.6 V are observed in the differential capacity curves of the Si–O–C anode, and they accounts for at least 50% of the total reversible capacity. It indicates some silicon species are electrochemically active with lithium and contribute the major part of the reversible capacity. By comparing ^{29}Si MAS NMR and Si (2p) XPS of the Si–O–C composite anode in the original, 10th fully lithiated, and 10th fully delithiated state, it can be concluded that the peaks are corresponding to SiO_2C_3, SiO_3C, and SiO_4 units. Their corresponding ^{29}Si MAS NMR resonances shift to high field and Si (2p) binding energies decrease when lithium is inserted, and both turn to the opposite direction when lithium is extracted. The SiO_4 resonances, comparing with that in the first cycle, decrease sharply in the tenth cycle. It indicates that parts of SiO_4 units are reversible while the others are irreversible with lithium. The reversible ones can change to Li–silicates (Li_2SiO_3) when lithium is inserted and transform backward to the original state when lithium is extracted. However, the irreversible ones transform to Li–silicate (Li_4SiO_4) in the discharge process, and cannot turn to the original state in the opposite direction.

The $SiOC_3$ units of the material disappear in the first discharge process and never recur during repeated cycles. Meanwhile SiC_4 units appear and exist in the following cycles. It indicates $SiOC_3$ units are totally irreversible with lithium. They could transform to SiC_4 when lithium is inserted, which are inactive with lithium and cannot transform back to $SiOC_3$ units when lithium is extracted.

Acknowledgement

We thank Ms. Li shun, Central South University of Forest and Technology, China, for support writing the paper.

References

[1] W. Xing, A.M. Wilson, G. Zank, J.R. Dahn, Solid State Ionics 93 (1997) 239–244.
[2] A.M. Wilson, G. Zank, K. Eguchi, W. Xing, B. Yates, J.R. Dahn, Chem. Mater. 9 (1997) 1601–1606.
[3] A.M. Wilson, G. Zank, K. Eguchi, W. Xing, J.R. Dahn, J. Power Sources 68 (1997) 195–200.
[4] A.M. Wilson, W. Xing, G. Zank, B. Yates, J.R. Dahn, Solid State Ionics 100 (1997) 259–266.
[5] A.M. Wilson, B.M. Way, J.R. Dahn, T.v. Buuren, J. Appl. Phys. 77 (1995) 2363–2369.
[6] L. Ning, Y. Wu, L. Wang, S. Fang, R. Holze, J. Solid State Electrochem. 9 (2005) 520–523.
[7] H. Fukui, H. Ohsuka, T. Hino, K. Kanamura, J. Power Sources 196 (2011) 371–378.
[8] H. Fukui, H. Ohsuka, T. Hino, K. Kanamura, ACS Appl. Mater. Interfaces 2 (2010) 998–1008.
[9] H. Fukui, H. Ohsuka, T. Hino, K. Kanamura, Chem. Lett. 38 (2009) 86–87.
[10] H. Konno, T. Morishita, C. Wan, T. Kasashima, H. Habazaki, M. Inagaki, Carbon 45 (2007) 477–483.
[11] H. Konno, T. Morishita, S. Sato, H. Habazaki, M. Inagaki, Carbon 43 (2005) 1111–1114.
[12] J. Shen, D. Ahn, R. Raj, J. Power Sources 196 (2011) 2875–2878.
[13] D. Ahn, R. Raj, J. Power Sources 195 (2010) 3900–3906.
[14] A. Saha, R. Rajw, D.L. Williamson, J. Am. Ceram. Soc. 89 (2006) 2188–2195.
[15] T.H. Xu, Q.S. Ma, Z.H. Chen, Mater. Lett. 65 (2011) 433–435.
[16] D.H. Everett, Pure Appl. Chem. 31 (1972) 577–638.
[17] W. Xing, J.S. Xue, T. Zheng, A. Gibaud, J.R. Dahn, J. Electrochem. Soc. 143 (1996) 3482–3491.
[18] G.D. Soraru, G. D'Andrea, R. Campostrini, F. Babonneau, G. Mariotto, J. Am. Ceram. Soc. 78 (1995) 379–387.
[19] G.D. Sorarh, G.D. Andrea, A. Glisenti, Mater. Lett. 27 (1996) 1–5.
[20] K.J.D. Mackenzie, M.E. Smith, Multinuclear Solid-state NMR of Inorganic Materials, First ed., Pergamon, 2002.
[21] J.F. Moulder, W.F. Stickle, P.E. Sobol, K.D. Bomben, Handbook of X Ray Photoelectron Spectroscopy: A Reference Book of Standard Spectra for Identification and Interpretation of Xps Data, second ed., Physical Electronics Division Eden Prairie, 1992.
[22] Q. Sun, B. Zhang, Z.-W. Fu, Appl. Surf. Sci. 254 (2008) 3774–3779.